Proceedings of the Control Conference Africa, 2021
Muldersdrift, South Africa, December 7-8, 2021

Experimental validation of three nonlinear MPP Solar tracking techniques

Y Gajadur and S Z Sayed Hassen
Department of Electrical and Electronic Engineering, Réduit, University of Mauritius
Email: yogindersing.gajadur@gmail.com

***Abstract*— Solar Photovoltaic Systems are required to operate at the Maximum Power Point (MPP) for efficient operation. In this work, the performance of three Maximum Power Point Tracking (MPPT) techniques namely Incremental Conductance (InCond), Extremum Seeking Control (ESC) and Particle Swarm Optimization (PSO) are compared experimentally. The ACOPower 20 W PV panel and associated drives are first modeled in Simulink together with the respective controllers, and for experimental validation, an Arduino Mega microcontroller was used as a digital platform to implement the different algorithms. The strengths and shortcomings of the proposed algorithms, as well as important attributes, related to the accuracy and difficulty to implement the proposed algorithms are highlighted and discussed. It was found that all three algorithms were able to successfully track the MPP and their performances were as expected from simulated results.**

Keywords---- Maximum Power Point Tracking, Incremental Conductance, Extremum Seeking Control, Particle Swarm Optimization.

I. INTRODUCTION

In the wake of rising energy demand and the growing concern for the adverse effects of global warming, the demand for renewable and clean energy technologies have been on the rise. Renewable energy sources include solar energy, wind energy and hydropower to name a few. Despite the fact that hydropower is the least expensive and is a more stable source of renewable energy, solar power is still more accessible and available almost anywhere in the world. In 2019, the National Renewable Energy Laboratory in Colorado developed a multi-junction concentrator solar cell capable of achieving a pinnacle efficiency of 47.1% [1]. High-end commercially available and affordable mono-crystalline PV cells still have efficiencies below 20 %.

The voltage across a PV panel varies non-linearly with the current through it. When the power of a uniformly irradiated PV panel is plotted against its voltage, a maximum power point is found to exist at a given voltage. The MPP is dynamic and shifts with variations in environmental parameters including irradiance and temperature but also with changing load. In PV systems equipped with bypass diodes, multiple local maxima can be observed under shadowing conditions. Operating away from the MPP decreases the efficiency of the system and MPP trackers are utilized for the continuous tracking of the MPP. The ability of DC-DC converters to perform load matching makes them suitable to be used as MPP trackers. In this work, a boost converter is chosen due to its higher efficiency as compared to other DC-DC converters [2].

The control signal for load matching is generated by a MPPT algorithm. The signal is a Pulse-Width Modulated (PWM) signal with the required duty-cycle and frequency. In the past decade, a multitude of MPPT algorithms were developed. These techniques vary in complexity, cost, speed of convergence, sensors required, hardware implementation, and effectiveness. Some common examples are the Perturb and Observe (P&O), Incremental Conductance (InCond), Fractional Open-Circuit Voltage (FOCV) and Hill Climbing (HC) techniques to name a few. Other more computationally complex MPPT algorithms include Fuzzy Logic Control (FLC), neural network, Particle Swarm Optimization (PSO) and hybrid PSO-FLC amongst others.

A previous study in [3] has demonstrated the performance of ESC using analog circuits and a switching PWM frequency of 300 kHz. The work in [4] has proven that PSO can also effectively track the MPP using a six-block hardware implementation setup.

This paper explores the performance of three MPPT algorithms namely: Extremum Seeking Control, Incremental Conductance and Particle Swarm Optimization using a low-cost experimental setup. The three algorithms are first simulated on a chosen PV system that is accurately modeled in Simulink and are shown to track the MPP. The algorithms are then validated on the experimental platform.

II. PHOTOVOLTAIC SYSTEM MODELING

As shown in Fig. 1, the proposed system consists of four main parts; a 20 W PV panel, a boost converter, a resistive load and the MPPT controller.

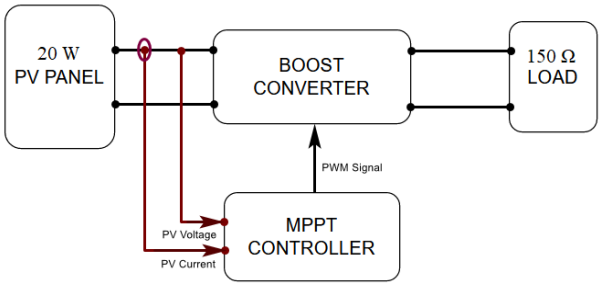

Fig. 1: Block diagram of proposed system.

A. Modeling of the PV Panel

Based on the single-diode model illustrated in Fig. 2, equation (1) that relates the output current to the photocurrent and voltage can be formulated as:

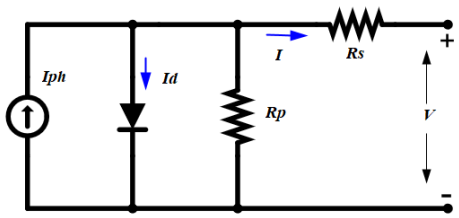

Fig. 2: Single-Diode model.

$$I = I_{ph} - I_{sat} \cdot \left(e^{\frac{V+I \cdot R_S}{\eta V_t}} - 1 \right) - \frac{V+I \cdot R_S}{R_p} \quad (1)$$

The photocurrent generated from incident photons is given as follows:

$$I_{ph} = I_{ph_{(STC)}} \cdot \frac{G}{G_{STC}} \cdot [1 + \alpha_1 \cdot (T - T_{STC})] \quad (2)$$

The unknown parameters V_t, I_{sat}, R_s and R_p are determined by the following set of equations:

$$V_t = \frac{k \cdot T}{q} \quad (3)$$

$$I_{sat} = C \cdot T^3 \cdot e^{-\frac{Egap}{kT}} \quad (4)$$

$$R_s \approx -\frac{dV}{dI}\Big| \; at \; v = v_{oc} \quad (5)$$

$$R_p \approx -\frac{dV}{dI}\Big| \; at \; I = I_{sc} \quad (6)$$

where I_{sat} is the diode's saturation current (A), η is the diode's ideality factor, C is the temperature coefficient (V/K), α_1 is the temperature coefficient of I_{sc} (A/K), T is the absolute temperature (K), k is the Boltzmann constant (1.3806503×10−23 J/K), E_{gap} is the band gap of semiconductor material (for crystalline silicon: E_{gap} = 1.124 eV = 1.8×10−19 J), G is the irradiance (W/m^2), I_{ph} is the photocurrent (A), q is the electronic charge (1.60217646×10−19 C), R_s is the series resistance (Ω), R_p is the parallel resistance (Ω), I is the panel's output current (A), V is the voltage at the terminals (V), V_{oc} is the open-circuit voltage (V), I_{sc} is the short-circuit current (A), STC are the standard test conditions of 1000 W/m^2 at 298.15 K.

Equations (1)-(2) are used to create the Simulink model shown in Fig. 3. The inputs are temperature and irradiance and the outputs are the terminal's current and voltage.

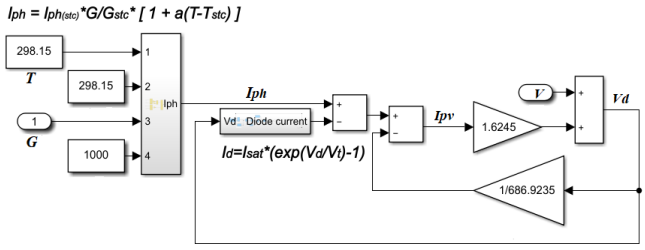

Fig. 3: Simulink block diagram representation of PV panel.

B. Validation of the PV Model

The respective I-V and P-V curve characteristics of the chosen PV panel are shown in Fig. 4

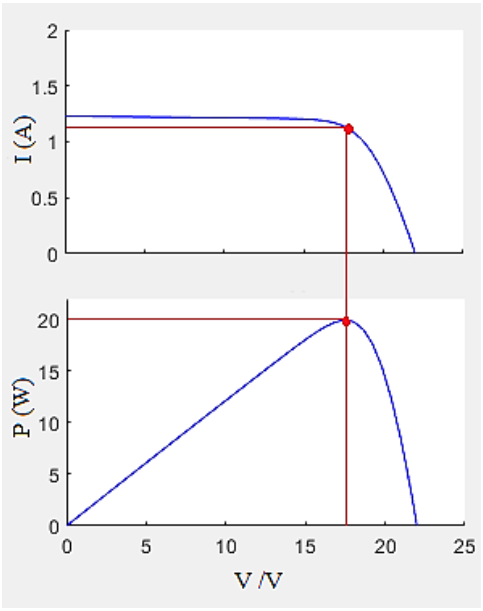

Fig. 4: Simulated I-V and P-V curves of the model.

To ensure a good representation of the actual system, we compare the datasheet values with the simulated values of the model. It was found that all simulated values were within 1 % of the datasheet values.

Table. 1: Comparison between Simulated and Datasheet values

	Simulated values	*Datasheet values*
I_{sc} (A)	1.23	1.23
V_{oc} (V)	21.7	22.0
MPP (W)	19.95	20.0
V_{mpp} (V)	17.66	17.50
I_{mpp} (A)	1.13	1.14

C. Boost converter design

The boost converter was designed to operate at a frequency of 31.372 kHz. This frequency is easily generated by the Arduino microcontroller. Given that continuous current is drawn from the panel and that the inductor's input current is the same current flowing through the panel, the parameters were chosen for the converter to work in Continuous Current Mode (CCM).

As stated in [5], the minimum value of inductance L, required to operate in CCM is calculated using equation (7):

$$L = \frac{D(1-D)^2 R_o}{2 \times f_s} \quad (7)$$

where L is the inductance (H), D is the duty cycle that yield a maximum L and R_o is the resistive load (Ω). In this analysis, a 1 mH inductor and 1 mF capacitors were used. The duty cycle required to operate at MPP is given by equation (8).

$$D = 1 - \sqrt{\frac{R_{eq}}{R_o}} \tag{8}$$

$$R_{eq} = \frac{V_{mpp}}{I_{mpp}} \tag{9}$$

where R_{eq} is the equivalent resistance at MPP (Ω), V_{mpp} is the MPP voltage (V) and I_{mpp} is the MPP current (A).

From equation (8), it can be deduced that R_{eq} cannot be greater than R_o for proper load matching. It is therefore important to choose a resistive load which is always greater than $R_{eq.}$ The value of R_{eq} at different irradiance levels are shown in Table 2. R_{eq} was found to be always lower than 150 Ω. Hence 150 Ω was used as an appropriate resistive load for the system.

Table 2. Calculation of R_{eq} at different irradiance.

Irradiation (kW/ m²)	V_{mpp} *(V)*	I_{mpp} *(A)*	$R_{optimum}$ *(Ω)*	P_{mpp} *(W)*	*Duty cycle (%)*
0.1	17.02	0.1147	148.4	1.952	0.5391
0.4	17.69	0.4588	38.56	8.117	49.30
0.7	17.71	0.7993	22.16	14.16	61.57
1.0	17.50	1.140	15.35	19.95	68.01
1.3	17.24	1.477	11.67	25.46	72.10

III. MAXIMUM POWER POINT TRACKING ALGORITHMS

In this section, we briefly explain the mode of operation of the three proposed MPPT algorithms.

A. Incremental Conductance

Incremental Conduction algorithm takes advantage of the fact that the gradient of the P-V curve can be calculated using current and voltage. At MPP the gradient is zero and can be expressed using equation (10).

$$\frac{dP}{dV} = 0 \tag{10}$$

The power can be calculated using current and voltage. Equation (10) can henceforth be written as equation (11).

$$\frac{dP}{dI} = \frac{d(V \times I)}{dI} = V + I\frac{dV}{dI} = 0 \tag{11}$$

Equation (11) is rearranged to obtain equation (12).

$$\begin{cases} \frac{dV}{dI} = -\frac{V}{I} & at\ MPP \\ \frac{dV}{dI} > -\frac{V}{I} & left\ of\ MPP \\ \frac{dV}{dI} < -\frac{V}{I} & right\ of MPP \end{cases} \tag{12}$$

The algorithm is described by the flowchart in Fig. 5.

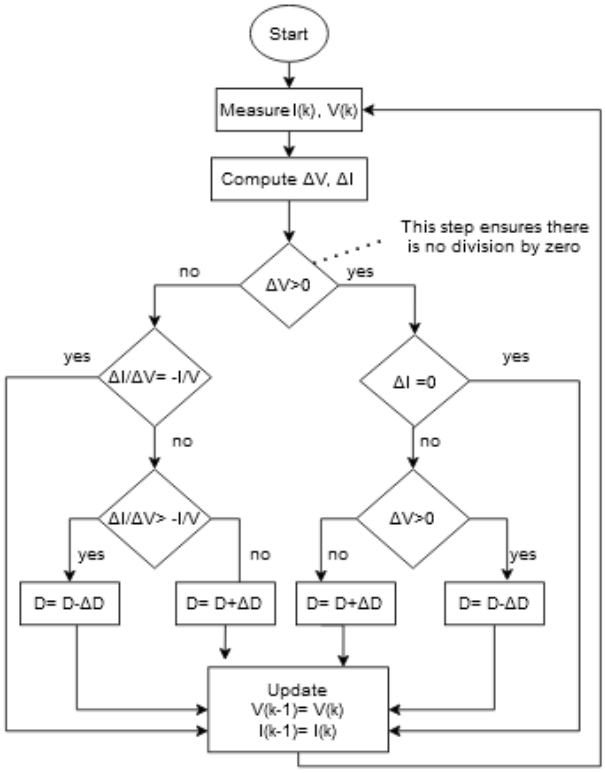

Fig. 5: Flowchart of InCond algorithm.

D is the current duty cycle, and ΔD is the step size. In this experiment, a step size of ΔD= (4/255) was empirically chosen to ensure reasonably sized oscillations in the power output at steady-state as well as fast-tracking time.

B. Extremum Seeking Control

Extremum Seeking Control seeks the change in phase angle between a dither and the response of the system to the dither to determine the region of operation. This is illustrated by Fig.6.

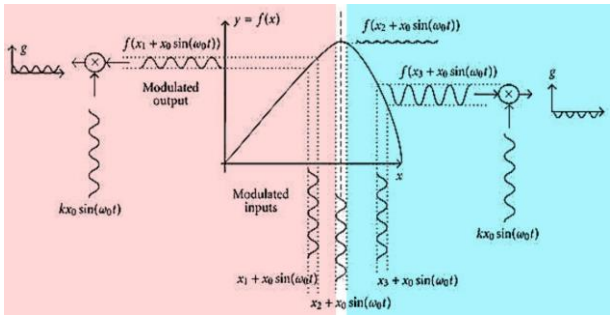

Fig. 6. Detection of region of operation using Extremum Seeking Control [3].

The modulated input is the disturbance that is introduced by the dither. By virtue of the positive gradient in the left region of the P-V curve (red region), the variation of the output power is in phase with the modulated input. In the right region, a negative gradient implies that a positive change in the modulated input would bring a negative change in power. Hence, a phase difference of 180° is observed between the modulated input and the power variation.

Using a high-pass filter, the AC variation in power can be extracted. The high-pass filtered signal, when multiplied with the modulated input signal, generates a positive DC signal g when operating in the left region. When operating in the right region, g is negative and at the MPP, g is alternating.

The signal g is smoothened using a low-pass filter to give an error signal e. Its value is a representation of the gradient at the operating point. e is fed into an integrator to drive the system to the MPP. This is illustrated by Fig. 7.

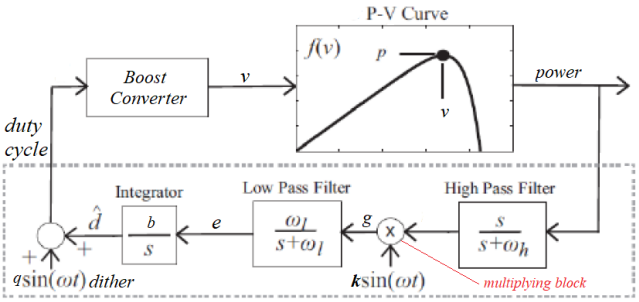

Fig. 7: Extremum Seeking Control [8].

In the PV system, the modulated input is the variation in voltage. This variation is introduced by the dither which is added to the duty cycle of the converter.

Mathematically, ESC can be described through equations (13)-(17). The power measured is expressed by equation (13).

$$P = f(V + a\sin(wt)) \tag{13}$$

Assuming that the dither is a small signal, P can be linearized at the operating point to obtain equation (14).

$$P \approx f(V) + \frac{df(V)}{dV} \cdot asin(wt) \tag{14}$$

The DC component $f(V)$ is removed by the high-pass filter and g can be expressed as equation (15) at the multiplying block.

$$g \approx \frac{df(V)}{dV} \cdot k \cdot a \cdot sin^2\,(wt) \tag{15}$$

Using the trigonometric identity $2sin^2(wt)=1-cos(2wt)$, equation. (15) is written as equation. (16).

$$g = \frac{1}{2}\frac{df(V)}{dV} \cdot k \cdot a - \frac{1}{2}\frac{df(V)}{dV} \cdot k \cdot a \cdot \cos\,(2wt) \tag{16}$$

Assuming that all the harmonics are filtered out by the low-pass filter, the error e is obtained. Equation (17) shows that e is proportional to the gradient of the P-V curve. $*$ is the convolution operator and L^{-1} stands for the inverse Laplace transform which represents the filter's impulse response [3].

$$e = \frac{1}{2}\frac{df(V)}{dV} \cdot k \cdot a * L^{-1}\{\frac{w_l}{s+w_l}\} \tag{17}$$

$f(V)$ is the PV power (W), a is the amplitude of the perturbed voltage from the boost converter which is assumed to be sinusoidal, k is the gain given to the dither at the multiplying block, w_l is the cutoff frequency of the low-pass filter (rad/s), w_h is the cutoff frequency of the high-pass filter (rad/s) , q is the dither's amplitude, b is the integrator's gain, w is the dither's frequency (rad/s) and s is the Laplace variable.

B.1 Parameter Values

Table 3 shows the values of all parameters used in the experiment. The cutoff frequencies and the different gains were fine-tuned by trial-and-error [6].

A dither of 200 Hz was used to ensure that there is no interference with the different frequencies present in the system as well as to achieve a quick response time. A phase lead of +10° was also added to the dither at the multiplying block to cancel out the lags introduced by different components in the system.

Table 3: Values of parameters used in the ESC controller

High-pass cutoff frequency (w_h)	6 rad/s
Low-pass cutoff frequency (w_l)	16 rad/s
Dither's frequency (w)	40 π rad/s
Dither's amplitude (q)	0.01
Phase lead introduced by the dither	+10°
Gain (k)	1000
Gain of integrator (b)	0.6

C. Particle Swarm Optimization

This technique is inspired by the way flock of birds naturally flies. Different agents, called particles are created and scattered over the solution space. In this case, the particles are evenly placed at different duty cycles. Each particle also has a corresponding power associated to its position. They are all given an initial velocity. As the particles move, the power associated to each one also varies. The best power attained by each particle (local best), and the best power attained in the whole swarm (global best) are stored in memory. After each iteration, the velocity of each particle is updated. A component in the direction of the local best power and a component in the direction of the global best power are added to the current velocity of the particles. After a number of iterations, all particles will have a tendency to converge towards the global best power, that is, the global MPP. Equations (18)-(19) describes how the velocities of the particles are updated.

$$v^i(k+1) = w^i v^i + c_1 r_1 \left(x^i_{best} - x^i(k)\right) + \quad c_2 r_2 \left(x_{gbest} - x^i(k)\right) \tag{18}$$

$$x^i(k+1) = x^i(k) + v^i(k+1) \tag{19}$$

From equation (18), the next velocity $v^i(k+1)$ of a particle comprises of the weighed initial velocity $w^i v^i$, a component towards the local best power given by the vector $\left(x^i_{best} - x^i(k)\right)$ and a component in the direction of the global best power given by the vector $\left(x_{gbest} - x^i(k)\right)$.

The new position $x^i(k+1)$ of each particle is calculated using its current position $x^i(k)$ and its newly calculated velocity $v^i(k+1)$. x is the duty cycle or position of the particle. $w^i$is the inertia of particle i, x^i_{best} is the best duty

cycle of particle i, x_{gbest} is the best duty cycle of the swarm, c_1 is a positive weight assigned to the direction towards the local best power, c_2 is a positive weight assigned to the direction towards the global best power and r_1, $r_2$are random values in the range [0, 1]. The values of parameters used experimentally are as follows; Number of particles N=10, Initial velocities=0 per sample,$c_1 = 0.3$, c_2= 0.9, $w^i = 0.1$, r_1, r_2 =*1,* and the particles are evenly scattered between 0.1<=D<=0.9.

Increasing $c_1$will place more emphasis on the particle to search around its local best solution. Increasing $c_2$will speed up all the particles towards the global best solution as more importance will be placed on the global best solution. The inertia given to each particle determines the rate at which its velocity can change. In this experiment, the parameters were determined by trial-and-error.

SIMULATION AND EXPERIMENTAL RESULTS

The system was simulated under an evenly distributed irradiance of 650 W/m^2. This irradiance level was estimated at that time of the day during the experiment using data obtained from the solargis website [7].

The model was simulated using a sampling time of 5µs. Upon measurement of the power using the microcontroller, it was found that a turnaround time of 40 ms was present which accounts for the time taken to acquire data from the sensor and to execute the codes. For a fair comparison of simulated results to that of the experiment, a similar delay was then introduced in the simulation. Hence, the MPPT block was placed in a subsystem running at a different sampling rate of 40 ms.

The experimental setup is shown in Fig. 8. Data acquisition for the voltage, current and power was realized using a single INA219 power sensor. Data measured were then logged into an SD card using the Arduino SD card module. The 5V PWM signal was converted into a 10V PWM signal using a driver to properly switch on the MOSFET in the converter.

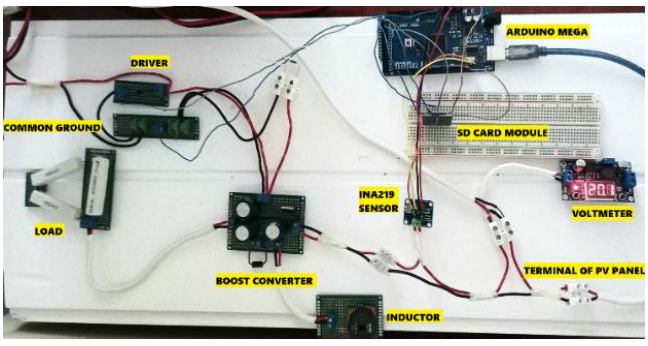

Fig. 8: Experimental setup

IV. RESULTS AND DISCUSSION

A. *Simulation results*

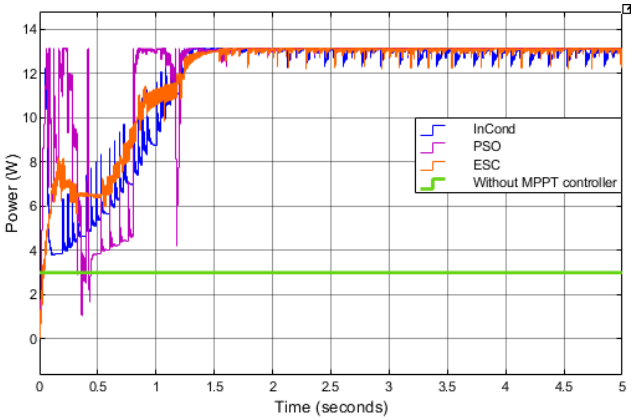

Fig. 9: Simulated power-time graph

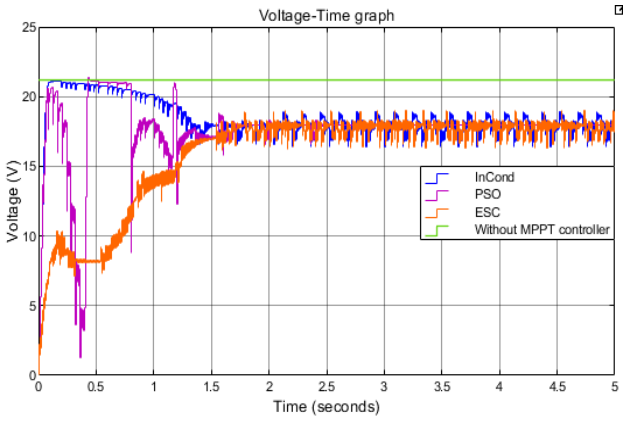

Fig. 10: Simulated voltage-time graph

B. *Experimental results*

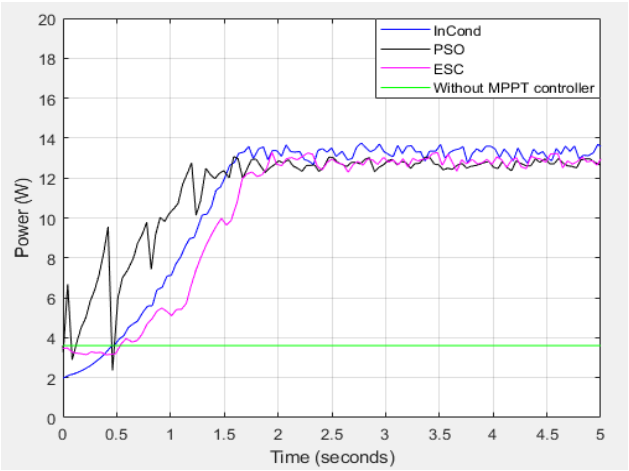

Fig. 11: Experimental power-time graph

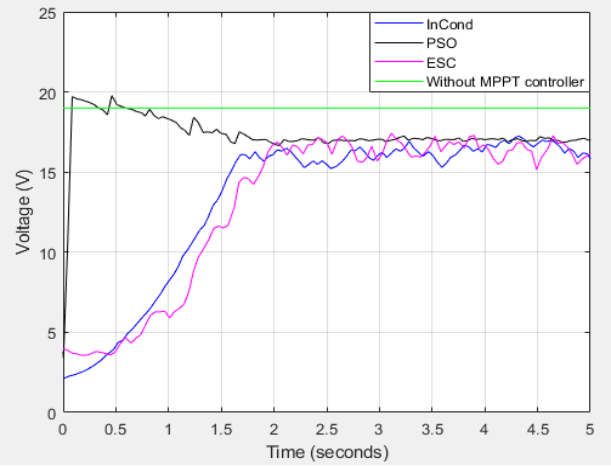

Fig. 12: Experimental voltage-time graph

C. *Comparison of simulated and experimental results*

Table 4: Values of performance indicators

Algorithm		*InCond*	*PSO*	*ESC*
Tracking time (s)	*Simulation*	1.325	1.277	1.537
	Experiment	1.728	1.588	1.942
Amplitude of oscillations (W)	*Simulation*	0.897	0.351	0.964
	Experiment	1.11	0.74	0.980
Power when load directly connected (W)	*Simulation*	3.00		
	Experiment	3.61		

Fig. 9 and Fig.11 shows the simulated and experimental power-time graphs respectively. The corresponding voltage-time graphs are shown in Fig. 10 and Fig. 12. In Table 4, we compare data obtained from experiment to that obtained from simulation.

It can be observed from Table 4 that the tracking times obtained in experiment were slightly higher than simulated values. This can be explained by the fact that delays introduced by different components, including the PWM driver, parasitic impedances and the MOSFET were neglected in simulation. It was also observed that due to parasitic impedances, the PWM signal was distorted and had smoother edges in the experiment. This might have affected the turning 'on' or 'off' times of the MOSFET and that could have also increased the tracking times. The oscillations seen experimentally at steady-state were also noted to be slightly higher than the simulated values. The MPPT controller were clearly effective and were able to bring about a 4-fold increase in power both in simulation and in the experimental setup. There are however no clear advantages of using one algorithm relative to the other and slight tuning the parameters of the controllers may alter the preferred choice of the user.

V. CONCLUSION

A 20 W photovoltaic system was modeled in the MATLAB/Simulink environment. The power extracted from the panel when a load is connected was compared to the power extracted when three different MPPT algorithms were simulated to drive the system to its MPP. The results obtained through simulation were then successfully validated on a low-cost experimental setup. It was shown that the Extremum Seeking Control, Incremental Conductance and Particle Swarm Optimization approaches could all successfully track the maximum power in PV systems. Furthermore, the Particle Swarm Optimization approach seems to offer better performance experimentally than the other two approaches but this may need to be validated with more rigorous testing using different parameter sets to tune the algorithms and using different platforms as well.

VI. REFERENCES

[1] John F. Geisz, Ryan M. France, Kevin L. Schulte, Myles A. Steiner, Andrew G. Norman, Harvey L. Guthrey, Matthew R. Young, Tao Song & Thomas Moriarty , "Six-junction III–V solar cells with 47.1% conversion efficiency under 143 Suns concentration," *Nature Energy,* p. 1, 2020.

[2] Pooja Sahu, Deepak Verma, Dr. S Nema., "Physical Design and Modelling of Boost Converter," Bhopal, India: Maulana Azad National Institute of Technology, 2016.

[3] R. Leyva, C. Olalla, H. Zazo, C. Cabal, A. Cid-Pastor, I. Queinnec, C. Alonso, "MPPT Based on Sinusoidal Extremum-Seeking Control in PV Generation," *International Journal of Photoenergy,* vol. 2012, pp. 1-7, 2012.

[4] Goncalo Calvinho, Jose Pombo, Silvio Mariano, Maria do Rosario Calado, "Design and Implementation of MPPT System Based on PSO Algorithm," in *International Conference on Intelligent Systems (IS)*, Funchal, Portugal, 2018.

[5] M. H. Rashid, Power Electronics Handbook, Pensacola, Florida: ACADEMIC PRESS, 2001.

[6] Y Tan, WH Moase, C Manzie, D Nesic, IMY Mareels, J Chen (ed.), "Extremum Seeking From 1922 To 2010," in *Proceedings of the 29th Chinese Control Conference 2010 | IEEE* , 2010.

[7] Solargis.com, 'Solar resource maps of Mauritius' [Online]. Available: https://solargis.com/maps-and-gis-data/download/mauritius. [Accessed 07 04 2020].

[8] Hadi Malek, Sara Dadras, YangQuan Chen, "An Improved Maximum Power Point Tracking Based on Fractional Order Extremum Seeking Control in Grid-Connected Photovoltaic (PV) Systems," in *ASME International Design Engineering Technical Conferences and Computers and Information in Engineering Conference*, Portland, Oregon, USA, 2013.